LIDSOR: A FILTER FOR REMOVING RAIN AND SNOW NOISE POINTS FROM LIDAR POINT CLOUDS IN RAINY AND SNOWY WEATHER

He Huang [1], Xinyuan Yan [1], Junxing Yang [1] *, Yuming Cao [1], Xin Zhang [1]

[1] School of Geomatics and Urban Spatial Informatics, Beijing University of Civil Engineering and Architecture, Beijing, China - huanghe@bucea.edu.cn, yan1075783878@126.com, yangjunxing@bucea.edu.cn, yyzyuming@126.com, zx2806404866@163.com

KEY WORDS: Autonomous Driving, LiDAR, Rainy and Snowy Weather, Point Cloud Denoising, Filter.

ABSTRACT:
As autonomous driving technology advances, ensuring the system's safety in rain and snow has emerged as a pivotal research topic. In rainy and snowy weather, rain and snow can generate noise points within the point cloud captured by the Light Detection and Ranging (LiDAR), significantly impeding the LiDAR's sensing capability. To address this problem, we first manually label the point cloud data gathered in rain and snow, categorizing all points into noise points and non-noise points. Subsequently, we analyze the intensity and spatial distribution characteristics of the rain and snow noise points and employ the gamma distribution curve to illustrate the spatial distribution characteristics of these noise points. Finally, we propose a Low-Intensity Dynamic Statistical Outlier Removal (LIDSOR) filter, an enhancement of the existing Dynamic Statistical Outlier Removal (DSOR) filter. Experimental results suggest that the LIDSOR filter can effectively eliminate rain and snow noise points while preserving more environmental feature points. Additionally, it consumes fewer computational resources. The filter we propose in this paper significantly contributes to the safe operation of the autonomous driving system in diverse complex environments.

1. INTRODUCTION

As autonomous driving technology continues to mature, the role of sensors in Autonomous Driving System (ADS) becomes increasingly critical. ADS integrates a diverse range of sensors, which collaboratively respond to a multitude of situations throughout the vehicle's driving process. Among these, LiDAR stands out as a central sensor within the autonomous driving perception system. It collects environmental data in the form of 3D point clouds. These point cloud data are processed to facilitate an array of advanced perception tasks integral to autonomous driving, such as semantic segmentation, object detection, and tracking. However, in rainy and snowy weather conditions, LiDAR tends to generate an abundance of noise points due to the occlusion and reflection of raindrops and snowflakes. This could potentially compromise the safety of ADS. To accommodate the use of autonomous driving technology in such inclement weather, the academic community has proposed numerous solutions to mitigate the issue of excessive noise points produced by LiDAR. Among these, implementing filters is a common approach. Traditional PCL-based generalized filters, such as Statistical Outlier Removal (SOR) filter and Radius Outlier Removal (ROR) filter (Rusu and Cousins, 2011), are able to eliminate some noise points produced by rain and snow. However, they tend to erase substantial environmental features. As a result, some researchers have proposed modifications like the Dynamic Statistical Outlier Removal (DSOR) filter (Kurup and Bos, 2021) and the Dynamic Radius Outlier Removal (DROR) filter (Charron et al., 2018), both of which take into account the variations in point density within the point cloud data. Additionally, following the successful application of intensity in point cloud classification, some researchers proposed a Low-Intensity Outlier Removal (LIOR) filter (Park et al., 2020) which integrated intensity into point cloud denoising. Another prevalent method is the use of Deep Learning (DL), as evidenced by the development of WeatherNet (Heinzler et al. 2020), the first CNN-based point cloud denoising method, and the more recent SunnyNet (Luo et al., 2022) and 4DenoiseNet (Seppänen et al., 2023). However, the generalizability of DL remains a considerable challenge due to the insufficient maturity of public datasets for severe weather.
To address these challenges, we propose an improved LIDSOR filter. This paper contributes in the following ways:

a) We performed a comprehensive statistical analysis on the intensity and spatial distribution characteristics of noise points generated in rain and snow, subsequently employing gamma curves for a more precise fitting of these noise point distribution characteristics.
b) We propose a LIDSOR filter. This filter is built on intensity and distance thresholds.
c) Our experimental results reveal that the LIDSOR filter outperforms existing filters in terms of overall efficacy.

2. RELATED WORK

2.1 Research Status of Severe Weather Datasets

Currently, publicly available severe weather datasets are not sufficiently mature. Below is a brief overview of severe weather datasets released in recent years. Bijelic et al. unveiled the DENSE dataset in 2020 (Bijelic et al. 2020). This multimodal severe weather dataset includes data captured under fog, snow, and heavy rain scenarios, with bounding boxes providing the labels. In 2021, Pitropov et al. released the Canadian Adverse Driving Conditions (CADC) dataset (Pitropov et al. 2021), marking the advent of the first autonomous vehicle dataset specifically tailored for adverse driving conditions. The CADC dataset utilizes the same annotation approach as the DENSE dataset and additionally offers time series information. In the same year, Kurup and Bos published a research paper addressing the removal of snow noise points (Kurup and Bos, 2021). Their contribution included the release of the Winter Adverse Driving DataSet (WADS), which is notably distinctive for containing data from snow days and for its point-by-point labeling. This dataset has significantly facilitated the study of snow noise removal, but it lacks time series information. In 2022, a research team introduced the Ithaca365 dataset (Diaz-Ruiz et al. 2022), encompassing diverse scenes (city, highway, countryside, campus) and weather conditions (snow, rain, sun). Its standout feature is the inclusion of road and object annotations, employing modal masks to document partial occlusions and 2D/3D bounding boxes. In 2023, the Boreas dataset was released by Burnett et al. (Burnett et al. 2023), encompassing over 350km of driving data. The Boreas dataset's unique strength lies in its data collection methodology: the same routes were driven repeatedly

* Corresponding author

over the course of a year. This approach resulted in the Boreas dataset housing comparable data.

2.2 Research Status of Point Cloud Denoising Methods

Denoising methods for point cloud data are generally divided into two primary categories: filter-based and DL-based methods. Filter methods tend to offer superior generalization and interpretability when compared to their DL counterparts. However, DL methods show a marked advantage when the task involves distinguishing noise points that are difficult to differentiate from non-noise points. Nevertheless, through algorithmic optimization, filters can effectively address this issue.

2.2.1 Research Status of Filter-Based Denoising Methods: Charron et al. proposed the DROR filter (Charron et al., 2018). In comparison to the ROR method, DROR can dynamically adjust the search radius, thereby retaining more environmental feature points at medium and long distances. Balta et al. proposed the Fast Cluster Statistical Outlier Removal (FCSOR) filter based on SOR (Balta et al., 2018). This method enhances algorithmic efficiency by implementing rapid cluster analysis subsequent to the downsampling of point cloud data. The intensity-based filtering method filters out rain and snow noise points by pre-setting LiDAR intensity thresholds for reflectors such as raindrops and snowflakes, and applying these thresholds to the intensity values (Hui et al., 2008). However, some environmental features and raindrops or snowflakes exhibit similar intensities, leading to potential misclassification by the filter. To overcome this limitation, Park et al. proposed the LIOR filter (Park et al. 2020) by merging the intensity filtering method and ROR. This approach sets a point cloud intensity threshold for initial filtering of the point cloud and subsequently applies ROR to the initial filtering results for secondary filtering. This compensates for the limitation of the singular attribute of the intensity filtering method. Kurup and Bos proposed the DSOR filter (Kurup and Bos, 2021), which optimizes the SOR filter by adaptively adjusting the thresholds in the SOR filter in line with the increase in LiDAR detection distance. Wang et al. proposed the Dynamic Distance-Intensity Outlier Removal (DDIOR) filter based on distance and intensity information (Wang et al., 2022). This method is specifically tailored to address the characteristics of snow noise points and takes both intensity information and distance into consideration, enabling effective filtering results in snowy weather. Duan et al. combined Principal Component Analysis and density clustering to propose the PCA-based adaptive clustering filtering (PCAAC) method (Duan et al. 2021). This is an improved method based on PCA that filters out sparse point cloud regions after transforming the 3D point cloud into two dimensions, thereby facilitating the removal of snowflake noise.

2.2.2 Research Status of DL-Based Denoising Methods: Sun et al. proposed a point cloud filtering method premised on a convolutional neural network model (Sun et al., 2019). This method is primarily designed to address the task of removing rain from individual images of urban street scenes for autonomous driving in rainy weather. Heinzle et al. advanced a point cloud filtering method based on a convolutional neural network deep learning framework (Heinzler et al., 2020). This method is capable of understanding the intrinsic data structure and generalizing its properties across different distances and clutter distributions. Further, it effectively incorporates the intensity information of the point cloud. Empirical results demonstrate that this method attains commendable filtering results in rainy weather.

3. APPROACH

3.1 Analysis of the Characteristics of Rain and Snow Noise Points

3.1.1 Data Collection: The equipment utilized for point cloud data acquisition in this study is the Hesai Pandar40 LiDAR. We annotate the collected point cloud data on a point-by-point basis. Figures 1 and 2 illustrate the visualization results of a frame point cloud, labelled point by point, in rainy and snowy weather, respectively. Noise points are represented by blue points, whereas non-noise points are indicated by red points. By analyzing these figures, it can be inferred that some noise points in rainy weather are situated below the ground plane and symmetrically arranged with respect to the above-ground features. These points are a result of the laser beam's reflection off the water on the ground. Conversely, in snowy weather, noise points predominantly occupy the spatial region above the ground plane and are highly concentrated near the LiDAR sensor. These points are generated by falling snowflakes reflecting the laser beam.

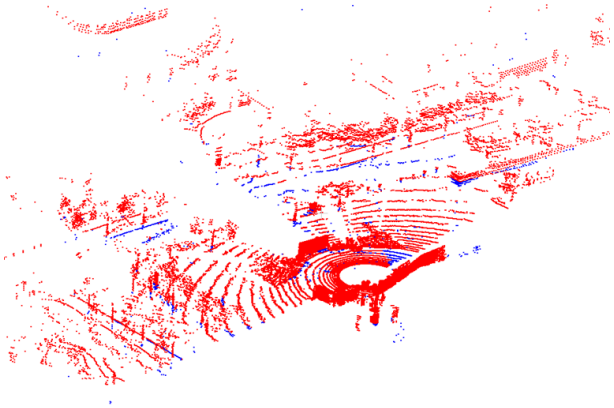

Figure 1. Visualization result of point cloud in rainy weather.

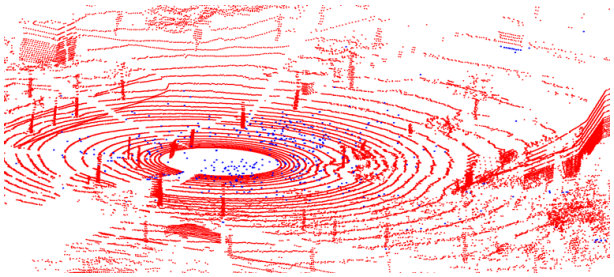

Figure 2. Visualization result of point cloud in snowy weather.

3.1.2 Analysis of the Characteristics of Rain Noise Points: We initially conducted a frame-by-frame statistical analysis of the labeled point cloud data in rainy weather. Figure 3 presents the results of this analysis for a specific frame in rainy weather. During this statistical analysis, for improved reader distinction, we color-coded noise points in red and non-noise points in blue.
In the statistical analysis of the relationship between intensity values and the number of points, the intensity values ranged from 0 to 255. A closer examination of Figure 3 a) demonstrates that the reflected intensity values of rain noise points occupy the lower range, and the count of noise points decreases as the intensity values increase. We calculated that in rainy weather, over 98% of rain noise points have intensities distributed in intervals of 25 units or less.
In our analysis of the relationship between distance intervals and the number of points, we initially partitioned the distance from

the point to the center of the LiDAR sensor into intervals of 10 meters. A more detailed observation of Figure 3 b) indicates that rain noise points are almost entirely concentrated within a 60m radius. To more effectively analyze the spatial distribution characteristics of noise points, we adopt a method from prior research: fitting the data to a gamma distribution curve (Ronnback and Wernersson, 2008). The Probability Density Function (PDF) of the gamma distribution is depicted in Equation (1). Figure 4 presents the gamma distribution fitting result for a point cloud frame in rainy weather. Table 1 showcases the parameter fitting results of the PDF for the gamma distribution corresponding to the rain noise points.

$$f(x) = \frac{\theta^k}{\Gamma(k)} x^{k-1} e^{-\theta x}, x > 0 \quad (1)$$

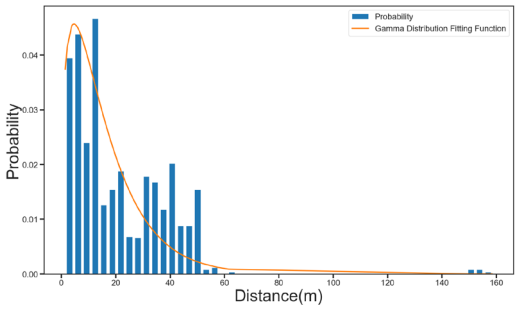

Figure 4. Gamma distribution fitting result for rain noise points.

Figure 4 illustrates that rain noise points exhibit significant outliers within some distance intervals. This is attributed to a large volume of noise points generated by water reflections from the road surface. These noise points produce anomalies in the count of rain noise points and interfere with the gamma distribution curve fitting process, subsequently reducing the fitting accuracy. This also explains why the variance of the gamma distribution curve parameter fitting results in rainy weather exceeds that in snowy weather. Upon a more detailed inspection of the fitted curves, it is observable that the quantity of rain noise points exhibits a tendency to initially increase and subsequently decrease. Notably, this variation manifests within a distance span of 0 to 20 meters.

Based on the LiDAR equation in Eq. (2) (Kashani et al. 2015), we understand that a point's intensity value is principally influenced by the object's reflectivity, the distance, and the angle of incidence. Consequently, we will statistically analyze the relationship between distance and intensity in the subsequent sections.

$$P_r = \frac{P_t D_r^2 \eta_{atm} \eta_{sys} \rho}{4R^2} cos\alpha_i \quad (2)$$

Fig 3 c) illustrates that rain noise points primarily cluster in the bottom-left corner. This pattern suggests the existence of a intensity threshold and a distance threshold specific to rain noise points, thus confirming the rationality of the methodological enhancement proposed in this paper.

3.1.3 Analysis of the Characteristics of Snow Noise Points: Following the process used to statistically analyze rain noise points, we also conducted a frame-by-frame analysis of the labeled point cloud data collected in snowy weather. The results of the statistical analysis of the point cloud in snowy weather are displayed in Figure 5. In line with prior research (Park et al., 2020) and Equation (2), it becomes apparent that when setting the intensity threshold for snow, we must consider the size of the snow particles, their reflectivity, and the ratio of the snow-covered area to the beam area. As the diameter of the snow increases, its reflectivity correspondingly decreases. In alignment with the LIOR paper (Park et al., 2020), we set the maximum diameter of snow at 1.12 cm, the angle of incidence at 45°, and the reflectivity of snow at 0.158 for this study.

Our statistical analysis of the relationship between the intensity values and the number of points, as shown in Figure 5 a), suggests that the intensity values of the noise points are almost entirely confined within an interval of 40 units. Further calculations revealed that in snowy weather, more than 98% of the snow noise points have their intensity distributed within an interval of 28 units.

Moving on to the statistical analysis of the relationship between the distance intervals and the number of points, Figure 5 c) demonstrates that the snow noise points are predominantly concentrated within a distance interval of 70m or less from the sensor's center, with the majority of the noise points being within 20m. In order to gain a more precise understanding of the spatial distribution characteristics of snow noise points, we fitted the data to a gamma curve. Figure 6 displays the result of fitting the gamma distribution to a point cloud frame in snowy weather. The fitting results for the parameters of the PDF of the gamma distribution corresponding to the snow noise points are detailed in Table 1. The fitting curves reveal that the snow noise points are mainly distributed within a spatial region 0-15m from the LiDAR sensor. The overall trend in the number of noise points displays an initial increase followed by a decrease, with changes occurring predominantly within the 5-10m range.

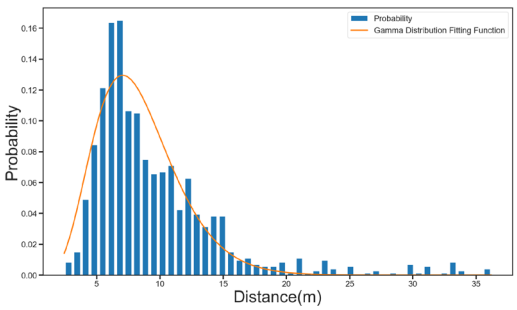

Figure 6. Gamma distribution fitting result for snow noise points.

Similar to the distance versus intensity characteristics for rain noise points, we note from Figure 5 c) that snow noise points are primarily concentrated in the lower left quadrant of the diagram. This observation confirms the appropriateness of the methodological enhancements made in this paper.

Table 1. Fitting results of gamma distribution PDF curve parameters.

Weather	Shape Parameter k	Scale Parameter θ	Variance r
Rain	1.410335	11.366825	0.738499
Snow	6.405399	1.304660	0.589831

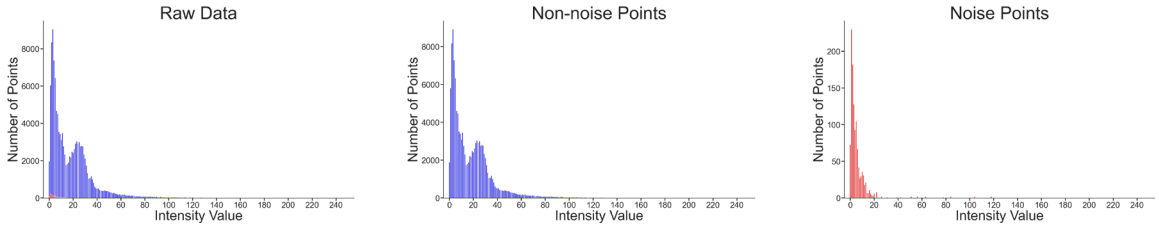

a) Relationship between intensity and number of points.

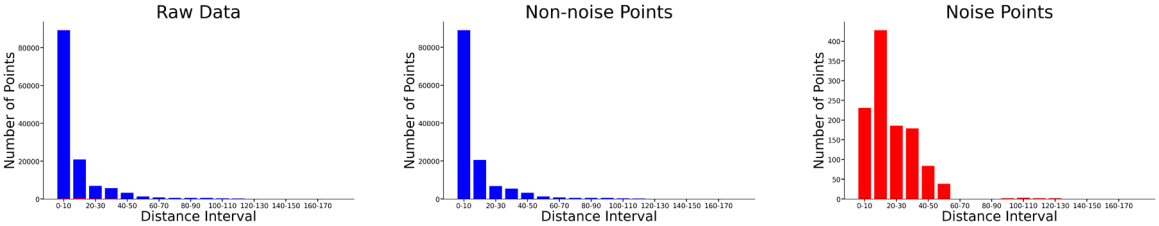

b) Relationship between distance intervals and number of points.

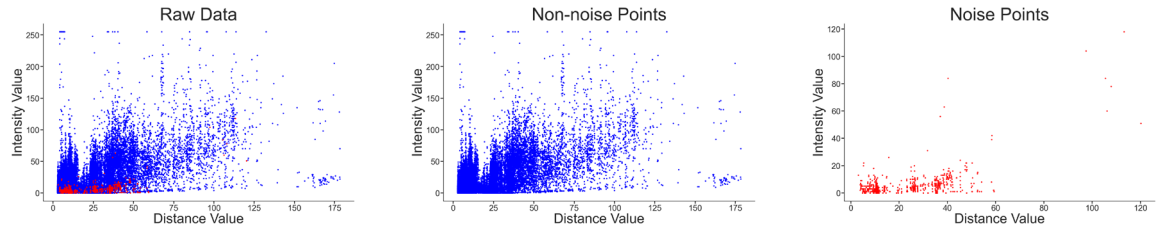

c) Relationship between distance and intensity.

Figure 3. Results of statistical analysis of point clouds in rainy weather.

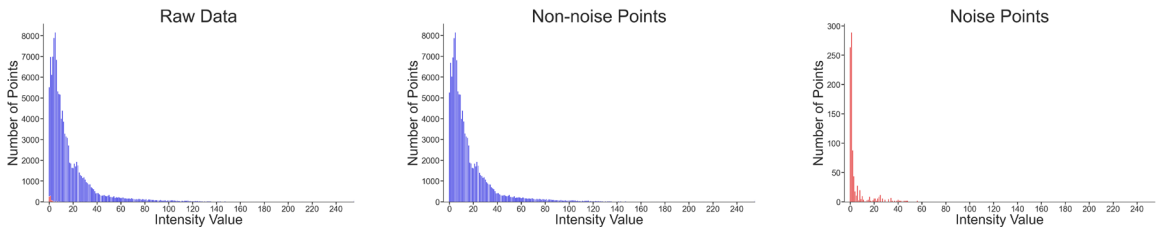

a) Relationship between intensity and number of points.

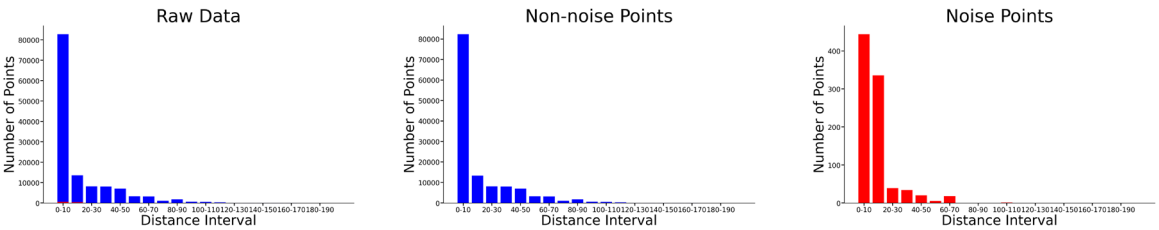

b) Relationship between distance intervals and number of points.

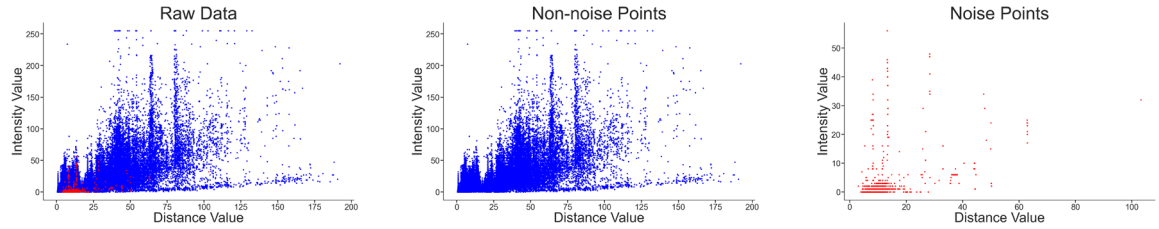

c) Relationship between distance and intensity.

Figure 5. Results of statistical analysis of point clouds in snowy weather.

3.2 Workflow and Basic Principle of Improved LIDSOR

3.2.1 Workflow of LIDSOR: The operational workflow of LIDSOR is bifurcated into two stages: initialization and filtering, as depicted in Figure 7. The initialization stage, executed only once before LIDSOR begins functioning, involves initial filtering using a state-of-the-art filter to identify noise points, followed by the computation of the gamma distribution fitting function. Subsequently, two input parameters—distance threshold and intensity threshold—are calculated according to Equations (3) and (4). Given the previously identified characteristics, we have set the intensity thresholds to 25 for rainy weather and 28 for snowy weather in this paper. Taking into account the lower probability in rainy weather, we establish a significance level at 0.01, suggesting that when the occurrence probability of rain and snow noise points falls below 0.01, the space can be considered noise-free. Following these significance test criteria, the distance thresholds for rainy and snowy weather with a P-value of 0.01 are approximately 30 meters and 16 meters, respectively. During the filtering stage, these computed distance and intensity thresholds are introduced as parameters into LIDSOR. This initiates operation and results in the production of filtered point cloud data.

$$T_d \Leftrightarrow f(T_d) = 0.01 \tag{3}$$

where $f(T)$ = the corresponding unit space distribution probability of point clouds at the respective distance

T_d = distance threshold

$$T_i \Leftrightarrow f(T_i) = N \tag{4}$$

where N = the unit space distribution quantity threshold, accounting for 2% of the total point cloud count

$f(T)$ = the corresponding unit space distribution quantity of point clouds for the respective intensity

T_i = intensity threshold

3.2.2 Basic Principle of LIDSOR: The LIDSOR pseudo-code is depicted in Algorithm 1. Distinct from DSOR, LIDSOR incorporates two additional input parameters: a distance threshold and an intensity threshold. The distance threshold regulates LIDSOR's filtering scope. Based on the characteristics results, the count of rain and snow noise points initially escalates and then declines with increasing detection distance. Hence, beyond a specific distance, the quantity of rain and snow noise points within the point cloud data becomes negligible. Setting a distance threshold enables LIDSOR to bypass filtering of these point clouds, thereby decreasing computational load and shortening algorithm filtering time.

The intensity threshold determines the intensity range filtered by LIDSOR. Given that rain and snow noise points exhibit a distinct intensity range, setting the intensity threshold instructs LIDSOR to process only those point clouds whose reflection intensities are comparable to the rain and snow noise points. Point clouds exhibiting considerable intensity differences from rain and snow noise points are exempted from filtering. This strategy preserves more environmental feature points from incorrect classification as noise and consequent removal by the filter, while also reducing computational load and filtering time.

Algorithm 1 Low-Intensity Dynamic Statistical Outlier Removal (LIDSOR) Filter

Input: Point Cloud $\boldsymbol{P} = p_i,\ i = 1,2,\dots,N;\ p_i=(x_i, y_i, z_i)$
$\boldsymbol{k} \leftarrow$ minimum number of nearest neighbors
$\boldsymbol{s} \leftarrow$ multiplication factor for standard deviation
$\boldsymbol{r} \leftarrow$ multiplication factor for range
$\boldsymbol{i} \leftarrow$ intensity threshold
$\boldsymbol{d} \leftarrow$ distance threshold

Output: Filtered Point Cloud $\boldsymbol{F} = f_i,\ i = 1,2,\dots,N;$ $p_i=(x_i, y_i, z_i)$

for $p_i \in P$ **do**
  calculate: $distance \leftarrow \sqrt{{x_i}^2 + {y_i}^2 + {z_i}^2}$
  if $distance < \boldsymbol{d}$ **then**
    primary filtrating point cloud $Q \leftarrow p_i$ (store in the primary filtrating point cloud)
  else
    $f_i \leftarrow p_i$ (stored in the filtered point cloud)
  end if
end for
$Q \leftarrow$ kd-tree pretreatment
for $p_i \in Q$ **do**
  mean distances $D \leftarrow$ nearestKSearch($\boldsymbol{k}$)
end for
calculate: mean $\mu \leftarrow D$
calculate: standard deviation $\sigma \leftarrow D$
calculate: global threshold $T_g \leftarrow \mu + \sigma \times \boldsymbol{s}$
for $p_i \in Q$ **do**
  calculate: $distance \leftarrow \sqrt{{x_i}^2 + {y_i}^2 + {z_i}^2}$
  calculate: dynamic threshold $T_d \leftarrow T_g \times \boldsymbol{r} \times d$istance
  if $D > T_d$ **and** $Intensity(p_i) < \boldsymbol{i}$ **then**
    $p_i \rightarrow$ discard (classified as noise)
  else
    $f_i \leftarrow p_i$ (stored in the filtered point cloud)
  end if
end for
return $\boldsymbol{F}$ (Output filtered point cloud)

4. RESULTS AND EVALUATION

In this paper, we conduct filtering experiments on point-by-point labeled point cloud data collected in rainy and snowy weather. We apply five existing filters - ROR, SOR, DROR, DSOR, DDIOR - as well as our proposed LIDSOR filter, each one separately. We undertake both qualitative and quantitative analysis of the experimental results. For the quantitative analysis, we employ accuracy, precision, recall, and filtering time as evaluation metrics.

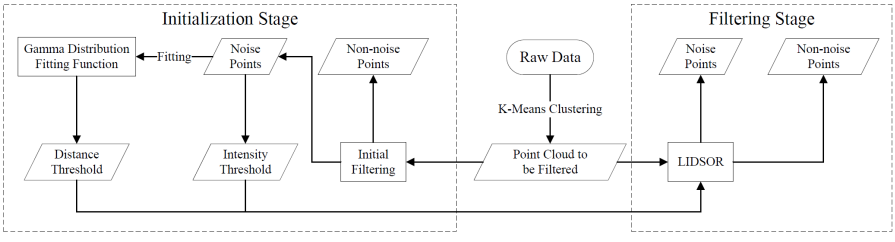

Figure 7. Workflow of LIDSOR.

4.1 Qualitative Analysis

Figures 8 and 9 present raw point cloud data for a frame in rainy and snowy weather, respectively. Visualization results of the point clouds, post-filtering by the six different filters under both weather conditions, are depicted in Figures 10 and 11. Analyzing these figures, we discern that the filtering algorithms of SOR and ROR, constrained by their principle, cannot adaptively adjust their constraints in line with detection distance. Consequently, these filters only retain environmental feature points at closer distances, while discarding mid to far distance points, resulting in a significant loss of environmental feature points. However, DROR, DSOR, DDIOR, and LIDSOR filters, capable of adaptively adjusting constraints based on detection distance, demonstrate notably improved filtering outcomes compared to ROR and SOR, successfully preserving a larger proportion of environmental feature points.

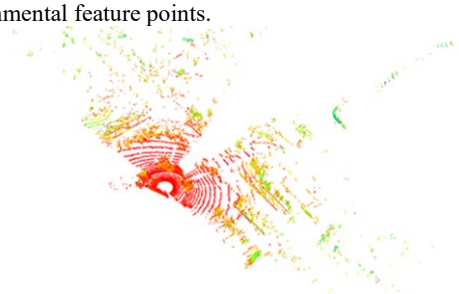

Figure 8. Visualization result of raw point cloud in rainy weather.

Figure 9. Visualization result of raw point cloud in snowy weather.

A further examination of Figures 10 c), d), e), and f) suggests that among the four methods, the DSOR filter demonstrates the least effective filtering outcome. While it succeeds in eliminating rain noise points, it also inadvertently discards significant environmental feature points, particularly those represented by leaves (blue boxes). The DROR filter, compared to the DSOR filter, manages to retain more environmental feature points at mid to far distances, though it falls short in effectively removing noise points at mid to near distances (green boxes). The DDIOR filter almost completely removes noise points and retains more environmental feature points at mid and far distances than the DSOR filter (purple boxes). The LIDSOR filter, impressively, manages to nearly eliminate all noise points while retaining the maximum number of environmental feature points, demonstrating the best filtering outcome among the four filters.
An analogous comparison of Figures 11 c), d), e), and f) indicates that the DROR filter retains more ambient feature points in snowy weather compared to the DSOR filter, particularly at mid and far distances (purple boxes). However, it doesn't perform as well as the DSOR filter at mid to short distances (blue boxes). At mid to near distances, the performance of the DDIOR and DSOR filters is quite similar, with both occasionally failing to remove individual noise points. Yet, at mid to far distances, the DDIOR filter preserves more ambient feature points (green boxes). The LIDSOR filter excels in denoising and retains ambient feature points exceptionally well.

4.2 Quantitative Analysis

4.2.1 Accuracy: The formula for the accuracy is shown in the following Equation:

$$Accuracy = \frac{TP + TN}{N} \tag{5}$$

where TP = The number of noise points recognized by the filter as noises
TN = The number of non-noise points identified by the filter as non-noise points
N = Total number of samples

Table 2 displays the accuracy results. In rainy weather, the DROR filter achieves the highest accuracy, with the LIDSOR filter following closely. However, the LIDSOR filter outperforms others in snowy weather. A deeper analysis indicates that the accuracy of every filter, barring ROR and SOR, is lower in rainy weather than in snowy weather. This suggests a diminished robustness of these filters in rainy weather as compared to their performance in snowy weather.

4.2.2 Precision and Recall: The formula for the precision is shown in the following Equation:

$$Precision = \frac{TP}{TP + FP} \tag{6}$$

where TP = The number of noise points recognized by the filter as noises
FP = The number of non-noise points recognized by the filter as noises

The formula for the recall is shown in the following Equation:

$$Recall = \frac{TP}{TP + FN} \tag{7}$$

where TP = The number of noise points recognized by the filter as noises
FN = The number of noise points identified by the filter as non-noise points

Table 2 presents the precision and recall outcomes for the six filters in rainy and snowy weather. The ROR and SOR filters sacrifice a substantial number of environmental feature points in rainy and snowy weather, thus reflecting low precision rates. A more detailed examination of the other four filters shows that the DROR filter, operating in rainy weather, records the lowest recall due to its domain search-based algorithm, failing to effectively eradicate non-sparse noise points generated by water reflections on the road surface. As an advancement, the LIDSOR filter significantly boosts precision while reducing recall relative to the DSOR filter, yet overall, it demonstrates the most balanced precision and recall rates among all filters. This balance suggests its capability to eliminate noise points whilst preserving as many environmental features as possible, thereby delivering high-quality point cloud data. In snowy weather, the DROR filter exhibits the strongest noise removal ability among the four, while the DDIOR filter struggles with retaining environmental features. As an improvement, the LIDSOR filter achieves an effective balance of precision and recall, outperforming the DSOR filter in retaining more environmental features.

a) Point cloud visualization result after ROR filtering.

b) Point cloud visualization result after SOR filtering.

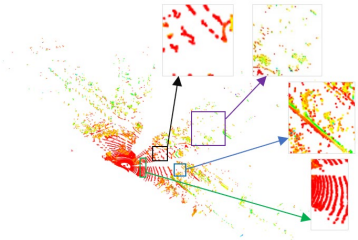

c) Point cloud visualization result after DROR filtering.

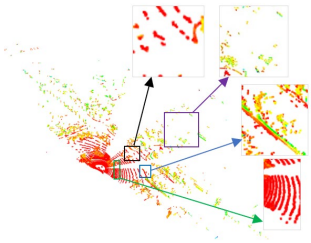

d) Point cloud visualization result after DSOR filtering.

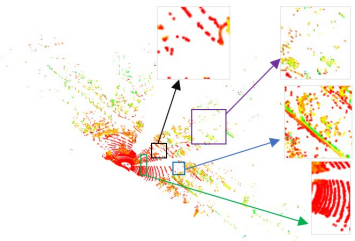

e) Point cloud visualization result after DDIOR filtering.

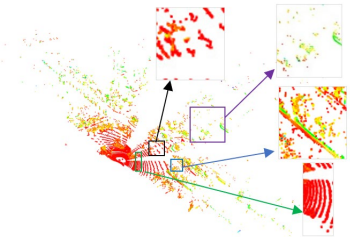

f) Point cloud visualization result after LIDSOR filtering.

Figure 10. Visual comparison of point cloud filtering results in rainy weather.

a) Point cloud visualization result after ROR filtering.

b) Point cloud visualization result after SOR filtering.

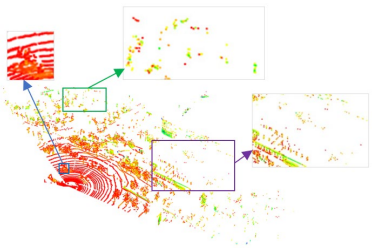

c) Point cloud visualization result after DROR filtering.

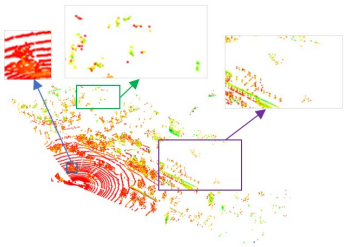

d) Point cloud visualization result after DSOR filtering.

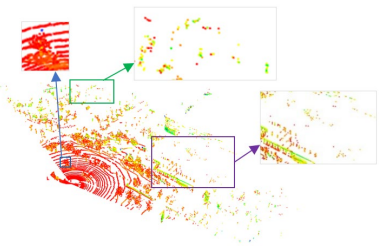

e) Point cloud visualization result after DDIOR filtering.

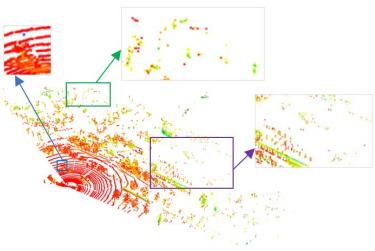

f) Point cloud visualization result after LIDSOR filtering.

Figure 11. Visual comparison of point cloud filtering results in snowy weather.

Table 2. Quantitative analysis results.

Filters	Rain				Snow			
	Accuracy	Precision	Recall	Time(ms)	Accuracy	Precision	Recall	Time(ms)
ROR	0.9053827	5.009	33.979	96.862	0.7401034	2.776	79.376	101.446
SOR	0.8470597	4.717	54.545	117.381	0.7797307	3.04	74.297	154.093
DROR	0.9831053	19.352	7.454	5284.036	0.9906161	52.618	68.808	4891.679
DSOR	0.9577436	8.546	22.441	105.250	0.9920792	61.235	62.608	143.596
DDIOR	0.9632657	10.216	18.525	105.155	0.9661649	21.063	64.653	165.484
LIDSOR	**0.9734935**	**10.276**	**12.373**	**104.907**	**0.993089**	**67.49**	**64.764**	**143.519**

4.2.3 Algorithm efficiency analysis: Table 2 reveals the average filtering time of the six filters for each frame point cloud in rainy and snowy weather. The ROR filter demonstrates the quickest filtering time, followed by the LIDSOR filter, while the DROR filter takes the longest, significantly exceeding the others. The superior efficiency of the ROR filter can be attributed to its lower algorithmic time complexity at O(*n*). The SOR, DSOR, and DDIOR filters, with a complexity of O(*logn*), are less efficient. The DROR filter's extensive filtering time stems from its methodological requirement to traverse all data points and conduct iterative radius searches, resulting in an algorithmic time complexity of O(*nlogn*), despite kd-tree preprocessing. The LIDSOR filter, an enhancement to the DSOR filter, shares the O(*logn*) complexity but manages to reduce filtering time due to the implementation of distance and intensity thresholds. These reduce computational demands and enhance algorithmic efficiency, especially as the volume of point cloud data increases.

5. CONCLUSION

In an effort to eliminate noise points caused by rain and snow within LiDAR point cloud data, we initially conduct an analysis of these noise points' unique characteristics. Our experimental findings demonstrate that the spatial distribution characteristics of these noise points can be proficiently defined using a gamma distribution fitting function. Subsequently, utilizing these characteristics, we propose a LIDSOR filter, which operates on the basis of intensity and distance thresholds. This innovative method incorporates two primary constraints: the intensity of the points and the detection range of the LiDAR sensor. By doing so, it capitalizes fully on both the intensity and spatial distribution characteristics of the noise points, thereby facilitating effective removal of noise points generated by rain and snow. Compared to existing filters, the filter we propose in this paper effectively retains a larger proportion of environmental feature points, ensures the elimination of noise points, and maintains real-time performance in rainy and snowy weather. The filter we propose in this paper significantly contributes to the safe operation of the autonomous driving system in diverse complex environments.

REFERENCES

Balta, H., Velagic, J., Bosschaerts, W., Cubber, G., D., Siciliano, B., 2018: Fast statistical outlier removal based method for large 3D point clouds of outdoor environments. IFAC-PapersOnLine 51(22), 348-353.

Bijelic, M., Gruber, T., Mannan, F., Kraus, F., Ritter, W., Dietmayer, K., Heide, F., 2020: Seeing through fog without seeing fog: Deep multimodal sensor fusion in unseen adverse weather. Proceedings of the IEEE/CVF Conference on Computer Vision and Pattern Recognition 11682-11692.

Burnett, K., Yoon, D., J., Wu, Y., Li, A., Z., Zhang, H., Lu, S., Qian, J., Tseng, W., Lambert, A., Leung, K., Y., K., Schoellig, A., P., Barfoot, T., D., 2023: Boreas: A multi-season autonomous driving dataset. The International Journal of Robotics Research 42(1-2), 33-42.

Charron, N., Phillips, S., Waslander, S., L., 2018: De-noising of lidar point clouds corrupted by snowfall. Conference on Computer and Robot Vision (CRV) 254-261.

Diaz-Ruiz, C., A., Xia, Y., You, Y., Nino, J., Chen, J., Monica, J., Chen, X., Luo, K., Wang, Y., Emond, M., Chao, W., L., Hariharan, B., Weinberger, K., Q., Campbell, M., 2022: Ithaca365: Dataset and Driving Perception Under Repeated and Challenging Weather Conditions. Proceedings of the IEEE/CVF Conference on Computer Vision and Pattern Recognition 21383-21392.

Duan, Y., Yang, C., Chen, H., Yan, W., Li, H., 2021: Low-complexity point cloud denoising for LiDAR by PCA-based dimension reduction. Optics Communications 482: 126567.

Heinzler, R., Piewak, F., Schindler, P., Stork, W., 2020: CNN-Based Lidar Point Cloud De-noising in Adverse Weather. IEEE Robotics and Automation Letters 5(2), 2514-2521.

Hui, L., Di, L., Xianfeng, H., Deren, L., 2008: Laser intensity used in classification of lidar point cloud data. IGARSS 2, II-1140-II-1143.

Kashani, A., G., Olsen, M., J., Parrish, C., E., Wilson, N., 2015: A review of LiDAR radiometric processing: From ad hoc intensity correction to rigorous radiometric calibration. Sensors 15.11 , 28099-28128.

Kurup, A., Bos, J., 2021: DSOR: A Scalable Statistical Filter for Removing Falling Snow from LiDAR Point Clouds in Severe Winter Weather. arXiv preprint arXiv:2109.07078.

Luo, Z., Ma, J., Xiong, G., Hu, X., Zhou, Z., Xu, J., 2022: Semantic Segmentation Based Rain and Fog Filtering Only by LiDAR Point Clouds. IEEE International Conference on Unmanned Systems (ICUS).

Park, J., I., Park, J., Kim, K., S., 2020: Fast and accurate desnowing algorithm for LiDAR point clouds. IEEE Access 8, 160202-160212.

Pitropov, M., Garcia, D., Rebello, J., Smart, M., 2021: Canadian adverse driving conditions dataset. The International Journal of Robotics Research 40(4-5), 681-690.

Ronnback, S., Wernersson, A., 2008: On filtering of laser range data in snowfall. IEEE 2, 17-33-17-39.

Rusu, R., B., Cousins, S., 2011: 3D is here: Point Cloud Library (PCL). IEEE international conference on robotics and automation 1-4.

Seppänen, A., Ojala, R., Tammi, K., 2023: 4DenoiseNet: Adverse Weather Denoising From Adjacent Point Clouds. IEEE Robotics and Automation Letters 8.1, 456-463.

Sun, H., Ang, M., H., Rus, D., 2019: A convolutional network for joint deraining and dehazing from a single image for autonomous driving in rain. IEEE/RSJ International Conference on Intelligent Robots and Systems (IROS) 962-969.

Wang, W., You, X., Chen, L., Tian, J., Tang, F., Zhang, L., 2022: A scalable and accurate de-snowing algorithm for LiDAR point clouds in winter. Remote Sensing 14(6), 1468.